Sensors & Actuators: B. Chemical 304 (2020) 127383

Contents lists available at ScienceDirect

Sensors and Actuators B: Chemical

journal homepage: www.elsevier.com/locate/snb

Electrochemical synthesis of phosphorus and sulfur co-doped graphene quantum dots as efficient electrochemiluminescent immunomarkers for monitoring okadaic acid

Jiawei Peng[a], Zixuan Zhao[a], Minli Zheng[a], Bingyuan Su[c], Xiaomei Chen[a,*], Xi Chen[b]

[a] College of Food and Biological Engineering, Jimei University, Xiamen, 361021, China
[b] State Key Laboratory of Marine Environmental Science, College of Chemistry and Chemical Engineering, Xiamen University, Xiamen, 361005, China
[c] Xiamen Center for Disease Control and Prevention, Xiamen, 361021, China

ARTICLE INFO

Keywords:
Electroysis
Phosphorus and sulfur
co- Doped
Graphene
Quantum dots
Okadaic acid
Electrochemiluminescence
Immunosensor

ABSTRACT

In this study, water-dispersed, uniform-sized phosphorus and sulfur co-doped graphene quantum dots (P, S-GQDs) were prepared by the one-step electrolysis of a graphite rod in an alkaline solution containing sodium phytate and sodium sulfide. Compared with GQDs and mono-doped GQDs (P-GQDs and S-GQDs), the P, S-GQDs dramatically improved the electrochemiluminescence (ECL) performance. Therefore, they were used as bright ECL signaling markers through conjugation with a monoclonal antibody against okadaic acid (anti-OA-MAb). Moreover, as an effective matrix for OA immobilization, the carboxylated multiwall carbon nanotubes-poly (diallyldimethylammonium) chloride-Au nanocluster (CMCNT-PDDA-AuNCs) composite promoted electron transfer and enlarged the surface area. Owing to the multiple amplifications, a competitive indirect ECL immunosensor for highly sensitive quantitation of OA has been developed. Under the optimized conditions, the 50% inhibitory concentration (IC_{50}) of the immunosensor was 0.25 ng mL^{-1}, and its linear range was 0.01–20 ng mL^{-1} with a low detection limit of 0.005 ng mL^{-1}. Finally, the proposed ECL sensor was successfully utilized to detect OA contents in mussel samples. Therefore, this study provides new insights into the designation of ECL luminophores and expands application of co-doped GQDs in fabrication of ECL immunosensors for shellfish toxin determination.

1. Introduction

As a main component of diarrhetic shellfish poison (DSP), okadaic acid (OA) can inhibit protein phosphatase activity, leading to hyperphosphorylation of the protein and thus affecting various biological functions of the organism [1,2]. Previous studies reported that OA is harmless in shellfish, with no influence on their taste, appearance, or smell; by contrast, it is harmful to humans, even at very low part-per-trillion doses [3]. As proposed by the European Food Safety Authority (EFSA), the maximum permitted level of OA in mussels was decreased from 160 to 45 μg kg^{-1} [4]. However, in many countries and areas, the permissible level of OA has still not been established. To minimize potential risk, development of a fast, reliable, and sensitive method to detect OA is of great importance. Recently, various immunosensors have been developed for OA quantitation, including chemiluminescence [3,5], differential pulse voltammetry [1,6,7], fluorescence [8], impedance [9,10], and square wave voltammetry [11]. Despite the rapid response and good selectivity of these methods, high background and poor controllability limit their vast application.

Electrochemiluminescence (ECL) is an ideal analytical method that combines the simplicity and controllability of electrochemistry with the high sensitivity, clear background, and wide linear range of chemiluminescence. To the best of our knowledge, no reports have demonstrated use of the immune-ECL technique to monitor OA. Furthermore, most of the reported ECL luminophores such as luminol [12], $Ru(bpy)_3^{2+}$ [13], CdSe [14], and CdTe [15] are poisonous, water-undispersed, or expensive. Therefore, designing and preparing new ECL luminophores as efficient immune-ECL markers remains a major challenge. Graphene quantum dots (GQDs), as a kind of zero-dimensional (0D) graphene, have not only outstanding electrochemical property similar with graphene [16–18], but also special luminescence property. In addition, GQDs behave low cytotoxicity and good biocompatibility, thus are attracted great attention in ECL sensors [19,20]. However, pristine GQDs without passivation have been demonstrated with low quantum yield (QY) and high electrooxidation potential, which hinder their practical application [21]. Fortunately, several recent reports

* Corresponding author.
E-mail address: xmchen@jmu.edu.cn (X. Chen).

https://doi.org/10.1016/j.snb.2019.127383
Received 19 August 2019; Received in revised form 14 October 2019; Accepted 4 November 2019
Available online 07 November 2019
0925-4005/

indicated that, based on theoretical calculations and experimental results, doping of GQDs with heteroatoms can greatly change their charge density distribution and band gap, thus improving their ECL performance [22]. Wang et al. reported that N-GQDs displayed superior ECL properties and could be used as a versatile signal indicator for ochratoxin A aptasensing [23]. In a recent report, Zhang et al. found that, by using $K_2S_2O_8$ as the co-reactant, the ECL efficiency of N, S-GQDs increased 5.8-fold, as compared to pristine GQDs [22]. Although ECL studies based on heteroatoms-doped GQDs are limited, most heteroatoms contain the element N, such as N-GQDs [24,25] and N, S-GQDs [22,26]. Since luminophores with advanced ECL activity and good biobinding ability play vital roles in improving the performance of ECL immunosensors, this study aimed to leverage advancements in N-doped GQDs-based ECL to synthesize additional co-doped GQDs and apply to ECL sensing of OA.

In this study, a green and facile electrochemical method was introduced to synthesize P, S-GQDs using a graphite electrode, sodium phytate, and sodium sulfide (Na_2S) as C, P, and S sources, respectively. Different from the traditional hydrothermal [25,27] and microwave methods [28], electrolysis owns advantages of mild conditions, good controllability and low cost. Based on our results, the resulting P, S-GQDs with a yellow-green photoluminescence emission revealed high ECL activity in the presence of $K_2S_2O_8$, and was therefore used as a bright signal indicator after monoclonal antibody-labeling against okadaic acid (anti-OA-MAb). To further improve the sensitivity of the OA sensor, carboxylated multiwall carbon nanotubes-poly(diallyldimethylammonium) chloride-Au nanocluster (CMCNT-PDDA-AuNCs) composite was used as the platform to immobilize OA. Owing to the multiple amplifications, a novel competitive indirect immunoassay for the highly sensitive monitoring of OA was developed through competition of P, S-GQDs marked anti-OA-MAb for free and immobilized OA. This study might prompt additional GQDs-based ECL studies and advance fabrication of ECL immunosensors for monitoring shellfish toxin.

2. Experimental methods

2.1. Reagents

OA potassium salt, anti-OA-Mab, and OA ELISA kits were obtained from Puhuashi Ltd. (Beijing, China). High-purity graphite rods with a 6 mm diameter were purchased from Gaoss Union Ltd. (Wuhan, China). Sodium phytate, Na_2S, $K_2S_2O_8$, Tween-20, $Ru(bpy)_3Cl_2$, PDDA, chitosan (CS), bovine serum albumin (BSA), tris(hydroxymethyl)aminomethane (Tris), N-hydroxy-succinimide (NHS), 2-(*N*-morpholino)ethanesulfonic acid (MES), and 1-ethyl-3-(3-dimethylaminopropyl) carbodiimide hydrochloride (EDC) were supplied by Sigma–Aldrich (Shanghai, China). Chloroauric acid ($HAuCl_4{\cdot}4H_2O$, 99.9%) was obtained from Aladin Ltd. (Shanghai, China). Carboxylated multiwall carbon nanotubes (CMCNT, diameter: 15 ± 5 nm, length: 0.5–2 μm, purity: 95%) were purchased from Tanfeng Tech. Inc. (Suzhou, China). Ultrapure water prepared by a Millipore Autopure WR600A (USA) was used throughout the study. Unless otherwise specified, all reagents used in the study were analytical grade.

2.2. Apparatus

The as-synthesized P, S-GQDs were characterized by transmission electron microscopy (TEM) (JEOL JEM-2100, Japan), dynamic light scattering (DLS) (Malvern instrument Ltd., UK), X-ray photoelectron spectroscopy (XPS, EscaLab-250Xi, Thermo Fisher Scientific, USA), UV-Vis absorption spectrophotometer (UV-2450, Shimadzu, Japan), fluorescence spectrometer (PerkinElmer-LS55, USA). The electrochemical (including electrochemical impedance spectroscopy (EIS) and cyclic voltammetry (CV)) and ECL tests were performed with an Autolab electrochemical workstation (PGSTAT302 N, Switzerland) and an MPI-A ECL analyzer (Remax Electronic Science & Technology Co. Ltd., China) (See more details in the ESI).

2.3. Electrochemical synthesis of P, S-GQDs

P, S-GQDs were synthesized via the one-step electrolysis of a graphite rod in a solution containing sodium phytate, Na_2S, and NaOH. Here, sodium phytate and Na_2S functioned as both the electrolyte and respective sources of P and S. The detailed synthesis process is as follows: 10 mL of 0.1 mol L^{-1} sodium phytate, 10 mL of 0.1 mol L^{-1} Na_2S, and 20 mL of 2 mol L^{-1} NaOH aqueous solution were first mixed as the electrolyte. Subsequently, a graphite rod and Pt foil, functioning as an anode and counter electrode, respectively, were inserted into the above solution. The voltage was set to 5.0 V, and the electrolysis lasted for 6 h. During the reaction, the electrolyte gradually turned to a brown and finally to a homogeneous black solution. The product was filtered using a 220 nm filter and further dialyzed using a 3500 Da dialysis bag for 48 h against pure water. Finally, the obtained product was treated by a vacuum freeze-drying process.

For comparison, monoatomic-doped GQDs (S-GQDs and P-GQDs) were prepared using the electrolysis method. The electrolytes were Na_2S and NaOH for the S-GQDs and sodium phytate for the P-GQDs. The other procedures were the same as those used in the preparation of P, S-GQDs.

2.4. Labeling of anti-OA-MAb to P, S-GQDs

Conjugation of anti-OA-MAb and P, S-GQDs was performed by a classic amidation reaction. Briefly, 180 μL of 7.5 mg mL^{-1} P, S-GQDs was dispersed in 500 μL of PBS solution (pH 7.4, 10 mmol L^{-1}) containing 50 mmol L^{-1} EDC and 25 mmol L^{-1} NHS. Next, the above solution was added into 680 μL of anti-OA-MAb (dilution of 1:500, 1:1000, and 1:2000 in pH 7.4, 10 mmol L^{-1} PBS). The mixture was incubated for 2 h at 4 °C. Subsequently, the resulting solution was centrifugated and washed with PBS (pH 7.4, 10 mmol L^{-1}) three times to remove residual anti-OA-MAb. To block non-specific binding sites, 400 μL of 2 wt% BSA containing 0.05% Tween-20 was added, and the solution was incubated at 4 °C for an additional 2 h. The obtained conjugation (named P, S-GQDs-Ab) was used as the ECL immunoprobe in the following tests.

2.5. Immobilization of OA on CMCNT-PDDA-AuNC-modified electrode

Scheme 1 illustrated the assembly process of the modified electrode. CMCNT was initially coated with PDDA according to a previous report [29]. Briefly, 5 mg CMCNT was mixed with 10 mL of 0.25% PDDA solution containing 0.5 M NaCl, followed by sonication of the mixture for 30 min to obtain a homogeneous black suspension. Subsequently, the complex was centrifuged and rinsed with water three times to remove the excess PDDA. Finally, 5 μL of 1 mg mL^{-1} CMCNT-PDDA was casted onto a polished glassy carbon electrode (GCE) and then dried at room temperature (RT, 25 °C).

AuNCs (using BSA as the template) were produced as described in previous reports [30,31], with some modifications. The as-synthesized AuNCs were immobilized on the CMCNT-PDDA GCE by immersing the electrode into AuNCs suspension and incubating for 30 min. Subsequently, the CMCNT-PDDA-AuNCs-modified GCE was rinsed with pure water and dried in N_2 atmosphere.

OA containing a carboxyl group was immobilized on the modified electrode through a classic amidation reaction [32]. First, the carboxylic group of OA was activated and incubated in a mixture containing 50 μL 0.2 mg mL^{-1} OA, 200 μL MES buffer (0.1 mol L^{-1}, pH 5.5), 50 mmol L^{-1} EDC, and 25 mmol L^{-1} NHS at RT for 1 h. Subsequently, 1 mL PBS (10 mmol L^{-1}, pH 7.4) was added to the mixture. As shown in Scheme 1, a CMCNT-PDDA-AuNCs-modified GCE was immersed in the activated OA solution and incubated for 1 h. Afterwards, the electrode was rinsed with 10 mmol L^{-1} PBS to remove the unbound

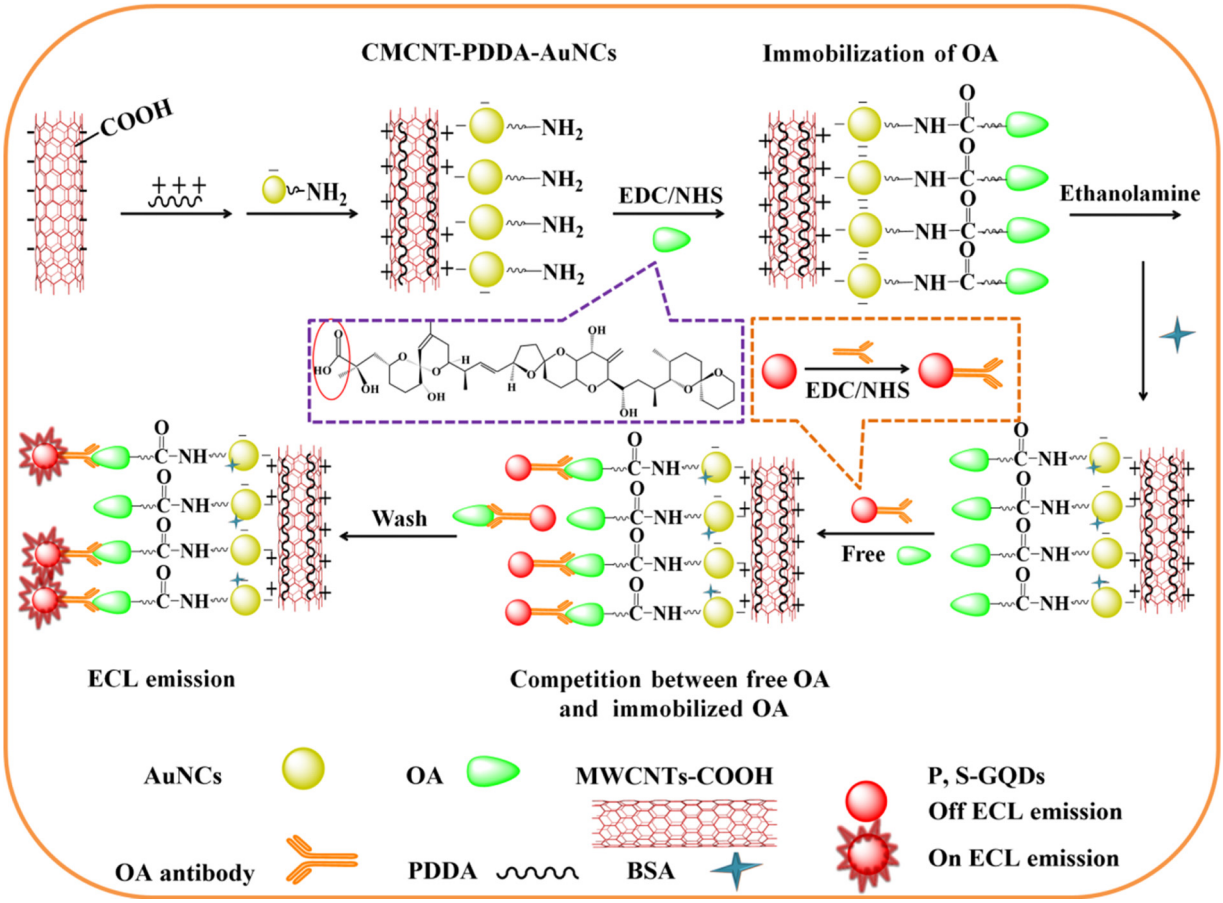

Scheme 1. Schematic representation for the fabrication and application of the immunosensor.

OA. It was then inserted in 1 mol L^{-1} ethanolamine solution for 1 h at RT to deactivate the remaining succinimine group. Afterwards, the modified electrode was rinsed with PBS and stored dry at 4 °C for further use.

2.6. ECL immunoassay for OA detection

First, the OA-CMCNT-PDDA-AuNCs GCE was incubated with 100 µL of 2 wt% BSA for 1 h at RT to prevent non-specific binding. Subsequently, 10 µL P, *S*-GQDs-Ab (dilution of 1:2, 1:5 and 1:10 in pH 7.4, 10 mmol L^{-1} PBS) and 10 µL OA standard solutions were casted onto the surface of the OA-CMCNT-PDDA-AuNCs-modified electrode in a fully wet environment to avoid vaporization during incubation. After incubating at 37 °C for 50 min, the electrode was rinsed with PBS containing 0.05% Tween-20 to remove physical adsorption. ECL measurements were performed in 50 mmol L^{-1} deoxygenated Tris-HCl buffer solution (pH 7.4) containing 0.1 mol L^{-1} $K_2S_2O_8$ and 0.1 mol L^{-1} KCl. ECL intensities of the immunosensor were detected with a photomultiplier tube voltage setting of -800 V. ECL peak intensity was recorded and plotted against the OA concentrations, and the 50% inhibition (IC_{50}) value and limit of detection (LOD) were determined according to the Sigmoidal curves.

2.7. Sample pretreatment

Non-contaminated mussels (*Ostrea plicatula*) purchased from the Jianong Market were treated according to a protocol described in a previous report [33]. Briefly, 2 g of non-contaminated mussels spiked with different concentrations of OA was extracted using 4.5 mL methanol: water (v:v = 80:20) for 10 min with shaking at 200 rpm and 37 °C. After centrifuging the crude extracts at 2000 rpm for 10 min, the supernatants were removed and diluted to 5 mL with ultrapure water. For hydrolysis, the diluted extract was mixed with 544 µL of 2.5 mol L^{-1} NaOH and then heated at 74 °C for 40 min. After cooling to RT, 432 µL of 2.5 mol L^{-1} HCl was added to neutralize the solution. Finally, a dilution step was carried out using PBS (pH 7.4, 10 mmol L^{-1}), and the final concentrations of spiked OA were 0.2, 0.4, and 0.8 ng mL^{-1}.

3. Results and discussion

3.1. Characterization of prepared P, S-GQDs

The water-dispersed P, S-GQDs in this study were prepared by the one-step electrolysis of a high-purity graphite rod in an alkaline solution containing sodium phytate and Na_2S. Except the precursors and electrochemical parameters, the alkaline condition was critical to form high-quality P, S-GQDs. In the absence of NaOH, the ECL efficiency (Φ_{ECL},%) of the as-prepared P, S-GQDs was calculated at 6.1% relative to the $Ru(bpy)_3Cl_2/K_2S_2O_8$ system, which is much lower than that obtained in the presence of NaOH (Φ_{ECL} of 39.5%) (Additional details for the Φ_{ECL} calculation are available in ESI). This suggests that more O and OH radicals serving as "scissors" are generated during the anodic oxidation of NaOH, thus facilitating P and S doping into the carbon structure of GQDs.

Fig. 1A presents representative TEM images of the P, S-GQDs. The ultrafine P, S-GQDs revealed a spherical shape and a homogeneous size of approximately 3.2 nm, which is consistent with the estimated size distribution results calculated from 100 particles (Fig. S1). XPS was used to study the composition of the as-prepared P, S-GQDs. As shown in Fig. 1B, four typical peaks located at 132.3, 167.2, 284.3, and 531.0 eV corresponded to the characteristics of P_{2p}, S_{2p}, C_{1s}, and O_{1s}, respectively. Additionally, based on the calculations, the atomic

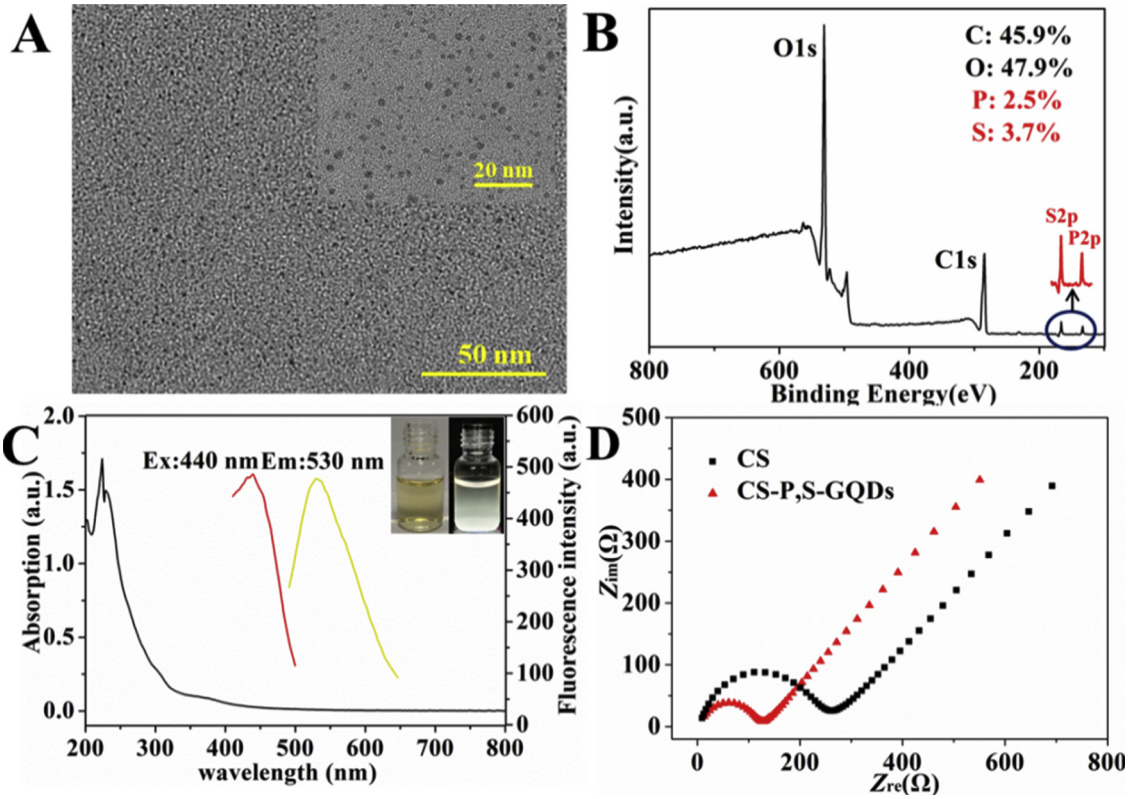

Fig. 1. (A) TEM image of the P, S-GQDs. (B) XPS spectra of the P, S-GQDs. (C) UV–vis absorption and fluorescence spectra of the P, S-GQDs. The inset displays photographs of the P, S-GQDs under daylight (left) and UV irradiation (right) in aqueous solution. (D) The EIS of P, S-GQDs/CS GCE and CS GCE.

percentages of the above four elements in the P, S-GQDs were 2.5%, 3.7%, 45.9% and 47.9%, respectively, demonstrating the successful doping of P and S into the framework of GQDs. The high resolution S_{2p} spectra in Fig. S2 A revealed four peaks at 163.4, 164.5, 168.5, and 169.8 eV. Referring to previous reports [34,35], the former two peaks were attributed to the C—S—C bond, and the latter two peaks were assigned to the C—$S(O)_2$—C sulfone bridges. The high resolution P_{2p} spectra (Fig. S2B) presented two main peaks at 131.8 eV and 133.5 eV related to the P—O and P—C bonds, respectively [36,37]. These results further confirmed that S- and P-based functional groups exist on the surface of P, S-GQDs. The optical property of P, S-GQDs was investigated by UV–vis absorption and fluorescence spectra, as shown in Fig. 1C. From the UV–vis absorption curve, a strong band centering at 235 nm and a weak band located at 290 nm were attributed respectively by π→π* transition (C = C) and n→π* transition (C = O(S)). The fluorescence results revealed that when the P, S-GQDs were excited at 440 nm, a maximum emission peak located at 530 nm could be observed. Accordingly, from the inset of Fig. 1C, the as-prepared P, S-GQDs appear pale orange under ambient daylight but yellow-green under a UV lamp (365 nm). These results suggested the successful synthesis of luminescent P, S-GQDs. Moreover, as both of the fluorescence and ECL related to the energy transition from excited state to ground state, the good fluorescence property of P, S-GQDs indicated the obtained P, S-GQDs were also a very promising ECL luminophores. Fig. 1D displays the EIS results of P, S-GQDs/CS GCE, and CS GCE in the solution containing 5.0 mmol L^{-1} $[Fe(CN)_6]^{3-/4-}$ and 1.0 mol L^{-1} KCl. It is evident that the electron transfer resistance of P, S-GQDs/CS GCE (170 Ω) was lower than that of CS GCE (280 Ω), suggesting faster interfacial charge transfer between the P, S-GQDs/CS GCE and electrolyte.

The electrochemical and ECL behaviors of P, S-GQDs/CS GCE were further studied. As shown in Fig. 2A, although there was a reduction peak on P, S-GQDs/CS GCE in the cyclic voltammograms, no ECL signal was observed on P, S-GQDs/CS GCE in the absence of $K_2S_2O_8$. Referring to the ECL of carbon nanodots [38], it is presumably due to the annihilation reaction of the cation radicals and anion radicals generated by P, S-GQDs. Conversely, in the solution containing $K_2S_2O_8$, the voltammograms revealed a current increase of the reduction peak at -1.35 V. Correspondingly, in the ECL intensity-potential (I_{ECL}-E) curve, a distinct cathodic ECL peak appeared on P, S-GQDs/CS GCE by scanning the potential in the negative direction. The onset luminescence occurred at -0.93 V, and the ECL rose sharply until reaching its maximum at -1.62 V. To further study the enhancement of the P, S-GQDs/$K_2S_2O_8$ system, the I_{ECL}-E curve on P, S-GQDs/CS GCE was compared to CS GCE, GQDs/CS GCE, P-GQDs/CS GCE, and S-GQDs/CS GCE. The amount of GQDs and doped-GQDs modified on every electrode was strictly controlled at 25 μg (10 μL, 2.5 mg mL^{-1}), and CS (5 μL, 0.01 mg mL^{-1}) was subsequently used to ensure these nanomaterials were tightly attached onto the GCEs. From the I_{ECL}-E curves presented in Fig. 2B, on the CS GCE, only a small ECL peak could be detected from $K_2S_2O_8$ itself. With the P, S-GQDs modification, a considerable increase (by a factor of ca. 7.8) in the ECL peak intensity was obtained, indicating that the enhanced ECL was due to the interaction between P, S-GQDs and $K_2S_2O_8$. In addition, we investigated the influence of different doping quantities of P and S on the ECL response of P, S-GQDs. The atomic percentages of P and S in different P, S-GQDs were calculated from the XPS results. As shown in Fig. S3, the ECL intensity of the P, S-GQDs changed as follows: $P_{2.5}$, $S_{3.7}$-GQDs (2.5% and 3.7% were the atomic percentages of the P and S elements in the P, S-GQDs) > $P_{2.3}$, $S_{1.3}$-GQDs > $P_{1.2}$, $S_{3.4}$-GQDs. This result indicated that the doping of P element has a more significant effect on the ECL intensity of P, S-GQDs than that of S element. According to the ECL emission mechanism of the reported GQDs/$K_2S_2O_8$ system [39], in this study, P, S-GQDs$^{\cdot-}$ and $SO_4^{\cdot-}$ were produced by the reduction of P, S-GQDs and $K_2S_2O_8$. Next, a hole from $SO_4^{\cdot-}$ was injected into the HOMO of P, S-GQDs$^{\cdot-}$ to generate an excited state of P, S-GQDs*, ultimately emitting the ECL signal (Scheme

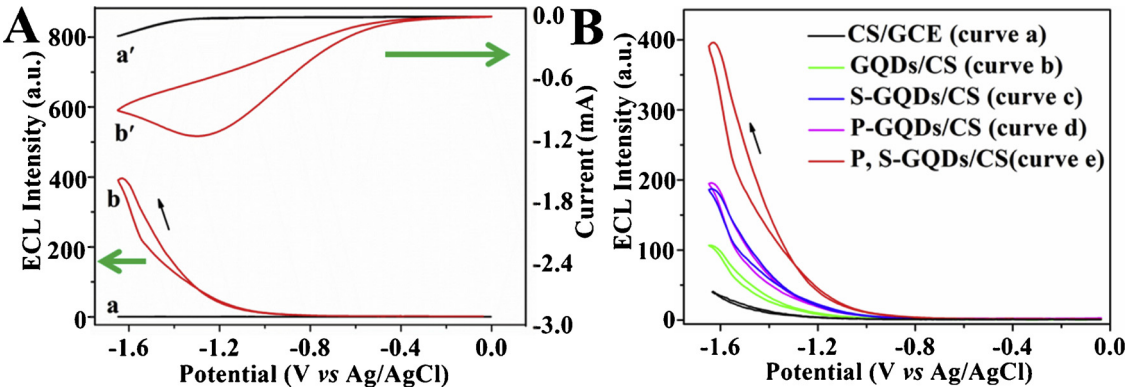

Fig. 2. (A) ECL emission curves and corresponding CVs of P, S-GQDs/CS GCE in the solution without (a and a,) and with (b and b,) $K_2S_2O_8$. (B) ECL emission curves of various modified GCEs in Tris-HCl buffer solution (0.5 mol L^{-1}, pH 7.4) containing 0.1 mol L^{-1} $K_2S_2O_8$ and 0.1 mol L^{-1} KCl.

S1). Additionally, the P, S-GQDs/CS GCE revealed the most positive onset potential and the highest ECL peak intensity among these electrodes, suggesting the superior ECL property of P, S-GQDs than the bare or mono-doped GQDs. The significant enhancement of ECL intensity may be ascribed to the abundant capturing centers of excitons produced on the surface of P, S-GQDs through efficient doping of P and S; thus, more holes from $SO_4^{\cdot-}$ could be captured, generating a brighter ECL by P, S-GQDs.

3.2. Characterization of OA-immobilized electrode and ECL immunoprobe

The assembly process of the OA-CMCNT-PDDA-AuNCs GCE is presented in Scheme 1. CMCNT-PDDA with positive charges was first modified on the GCE surface. Afterwards, AuNPs with a uniform size of ca. 2.5 nm and negative charges (Fig. S4) were fixed on the surface of CMCNT-PDDA by an electrostatic interaction. In comparison against the CMCNT-PDDA morphology (inset of Fig. 3A), the AuNPs were well dispersed on the surface of CMCNT-PDDA. The final step was OA immobilization on the surface of the modified electrode. Following surface activation with EDC/NHS, a classic amidation reaction occurred between the activated carboxylic group of OA molecules and the amine group of BSA around AuNPs, thus producing the OA-CMCNT-PDDA-AuNCs GCE. EIS is an effective tool to monitor impedance changes of the electrode surface during the modification process. Fig. 3B displays the EIS results of bare GCE, CMCNT-PDDA GCE, CMCNT-PDDA-AuNCs GCE, and OA-CMCNT-PDDA-AuNCs GCE in a 5.0 mmol L^{-1} $[Fe(CN)_6]^{3-/4-}$ solution containing 1.0 mol L^{-1} KCl. As depicted, the CMCNT-PDDA GCE and CMCNT-PDDA-AuNCs GCE showed a much lower resistance than bare GCE (161.2 Ω), resulting in the good electric conductive ability of CMCNT and AuNCs, which is consistent with previous reports [40]. After OA immobilization, a significant increase in electron transfer resistance (189.4 Ω) was observed, as compared to CMCNT-PDDA GCE and CMCNT-PDDA-AuNCs GCE, but similar to bare GCE. This result demonstrated that although conductivity of the OA molecule is poor, after combining with CMCNT-PDDA-AuNCs, GCE conductivity was hardly affected after modification. Based on these observations, the OA-CMCNT-PDDA-AuNCs GCE enables fast electron transfer on the electrode/solution interface, which is important for the development of ECL sensors.

The ECL immunoprobe of P, S-GQDs-Ab was prepared by an amidation reaction between anti-OA-MAb and P, S-GQDs. To verify formation of the bioconjugate, UV–vis absorption, DLS, and ECL measurements were applied for product characterization. As shown in Fig. 4A, the UV–vis absorption peak of anti-OA-MAb was located at 280 nm, which is attributed to the π-π* transition between tryptophan and tyrosine residues of the proteins [41]. After combining with P, S-GQDs, a slight blue shift (~10 nm) appeared on the UV–vis absorption peak of P, S-GQDs-Ab, which might be due to the influence of the local dielectric environment of P, S-GQDs towards anti-OA-MAb [42]. In addition, from the DLS result, the size of P, S-GQDs-Ab was calculated as 1958 nm, which is close to the sum of the particle sizes of P, S-GQDs (552.2 nm) and anti-OA-MAb (1558.1 nm), indicating successful preparation of the P, S-GQDs-Ab bioconjugate. Here, it should be noted that the hydrodynamic diameter measured by DLS is larger than that obtained by SEM or TEM, because the hydrodynamic diameter of the nanoclusters is the hydrated diameter obtained by combining the nanoparticle cores together with the solvent coating layer, while for SEM or TEM, this hydration layer is not present. Furthermore, the ECL

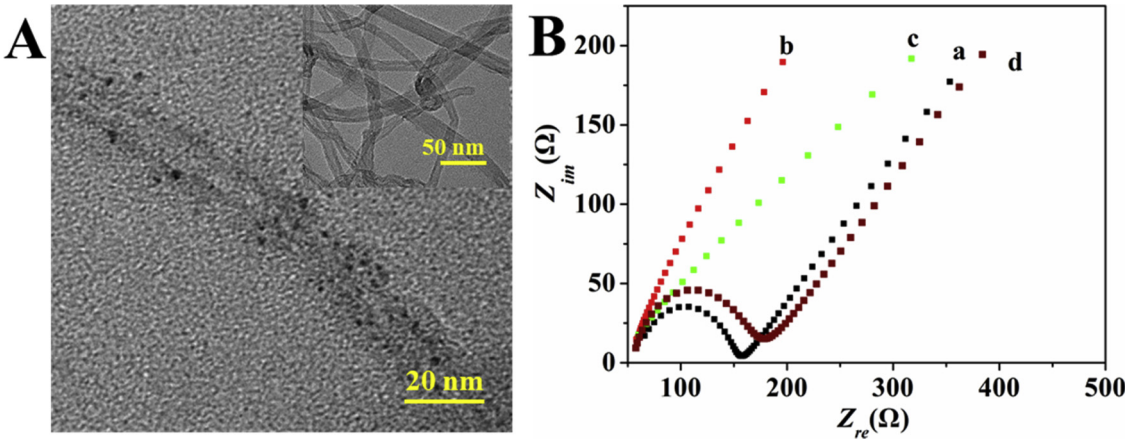

Fig. 3. (A) The TEM image of CMCNT-PDDA-AuNCs. The inset displays the TEM image of CMCNT-PDDA. (B) EIS results of bare GCE (a), CMCNT-PDDA GCE (b), CMCNT-PDDA-AuNCs GCE (c) and OA-CMCNT-PDDA-AuNCs GCE (d) in a 5.0 mmol L^{-1} $[Fe(CN)_6]^{3-/4-}$ solution containing 1.0 mol L^{-1} KCl.

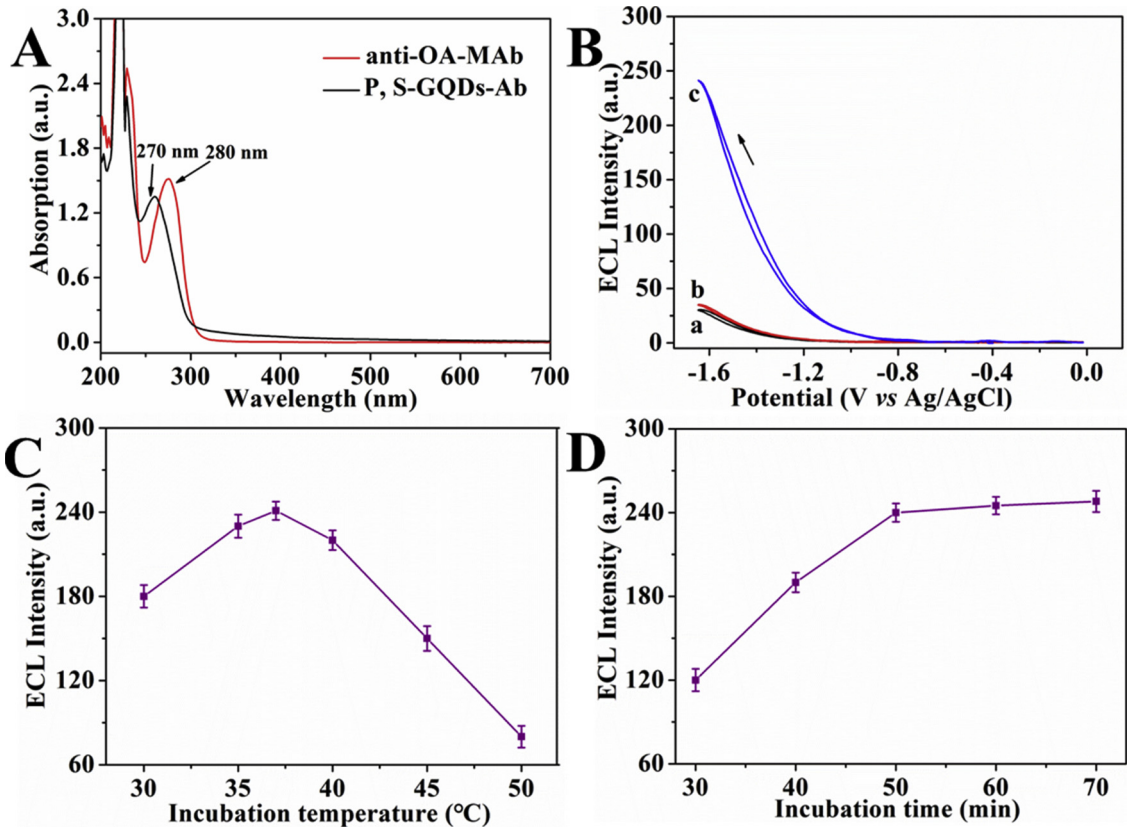

Fig. 4. (A) UV–vis absorption spectra of anti-OA-MAb and P, S-GQDs-Ab. (B) ECL emission curves of the OA-CMCNT-PDDA-AuNCs GCE (a), the OA-CMCNT-PDDA-AuNCs incubated in P, S-GQDs (b) and P, S-GQDs-Ab solution (c). (C) Effects of the incubation temperature and (D) incubation time on the ECL peak intensity of the immunosensor.

behaviors of OA-CMCNT-PDDA-AuNCs GCE before and after incubation in the P, S-GQDs-Ab and P, S-GQDs solutions were studied and compared. As depicted in Fig. 4B, the OA-CMCNT-PDDA-AuNCs GCE itself revealed a small ECL peak, similar to of CS GCE mentioned in Fig. 2B. During incubation in the P, S-GQDs solution, only a slight increase was observed on the OA-CMCNT-PDDA-AuNCs GCE, indicating that the amount of non-specific absorption of P, S-GQDs on the modified electrode was small and could be ignored. Further, after incubation in P, S-GQDs-Ab, the specific affinity between OA and anti-OA-MAb generated an abundant amount of modified P, S-GQDs-Ab on the electrode surface, resulting in a significant increase (~6.9 times) of the ECL peak intensity. This result further supported the successful synthesis of P, S-GQDs-Ab.

As the binding amount of the ECL immunoprobe on the surface of the electrode plays an important role in the sensitivity of the ECL immunosensor, the incubation conditions of OA-CMCNT-PDDA-AuNCs GCE in P, S-GQDs-Ab solution have been optimized. Fig. 4C demonstrated that an incubation temperature that was too high or too low did not facilitate interactions between OA and anti-OA-MAb. When the electrode was incubated in P, S-GQDs-Ab solution at 37 °C, the highest ECL peak intensity was obtained, indicating the largest amount of P, S-GQDs-Ab binding on the electrode. The effect of incubation time (30–70 min) on the ECL signal was also investigated. As presented in Fig. 4D, the ECL intensity grew with increases in incubation time during the first 50 min, which then reached saturation. To decrease the detection time and improve efficiency of the ECL immunosensor, a time period of 50 min was chosen for the incubation stage.

3.3. Determination of OA

A novel competitive indirect ECL immunoassay based on the competition of P, S-GQDs-Ab for free and immobilized OA was developed and optimized. As shown in Scheme 1, if the amount of free OA increased, immunoprobe linking to the immobilized OA was decreased, leading to the decrease of ECL intensity; conversely, less free OA would result in the increase of ECL intensity. Thus, from the competitive indirect ECL immunosensor, the amount of free OA can be determined. Fig. 5A presents representative I_{ECL}-E curves of OA-CMCNT-PDDA-AuNCs GCE incubated in P, S-GQDs-Ab solution without and with 1 ng mL^{-1} and 5 ng mL^{-1} of OA. As expected, the binding between P, S-GQDs-Ab and free OA caused less P, S-GQDs-Ab immobilization on the electrode surface, resulting in decreased ECL intensity. Moreover, the ECL intensity showed sensitivity towards the OA concentration due to decreases in ECL intensity with accumulation of free OA. This phenomenon further confirmed the feasibility of the proposed ECL immunosensor to monitor OA with high sensitivity.

To create an effective ECL immunoassay with high performance for OA detection, the possible affecting factors, including the dilution of anti-OA-MAb and P, S-GQDs-Ab, were optimized. Previous studies suggest that larger amounts of antibody lead to stronger signal intensity, but lower sensitivity of immunoassays [33]. Thus, a compromise between a good ECL response and high sensitivity should be considered to determine the optimal antibody amount. Figs. 5B and 5 C display the calibration curves under different dilution ratios of anti-OA-MAb and P, S-GQDs-Ab, respectively, which show significant decreases in the IC_{50} values as the antibody dilution ratio increased. As calculated from Fig. 5B, corresponding to the dilution ratios of anti-OA-MAb at 1:500, 1:1000, and 1:2000, the IC_{50} values were 1.06 ng mL^{-1}, 0.45 ng mL^{-1}, and 0.25 ng mL^{-1}, and the LOD values (corresponding to 85% antibody binding) were 0.050 ng mL^{-1}, 0.009 ng mL^{-1}, and 0.005 ng mL^{-1}, respectively. With further increases in the dilution ratio, the decrease in the ECL response was negligible. Similar

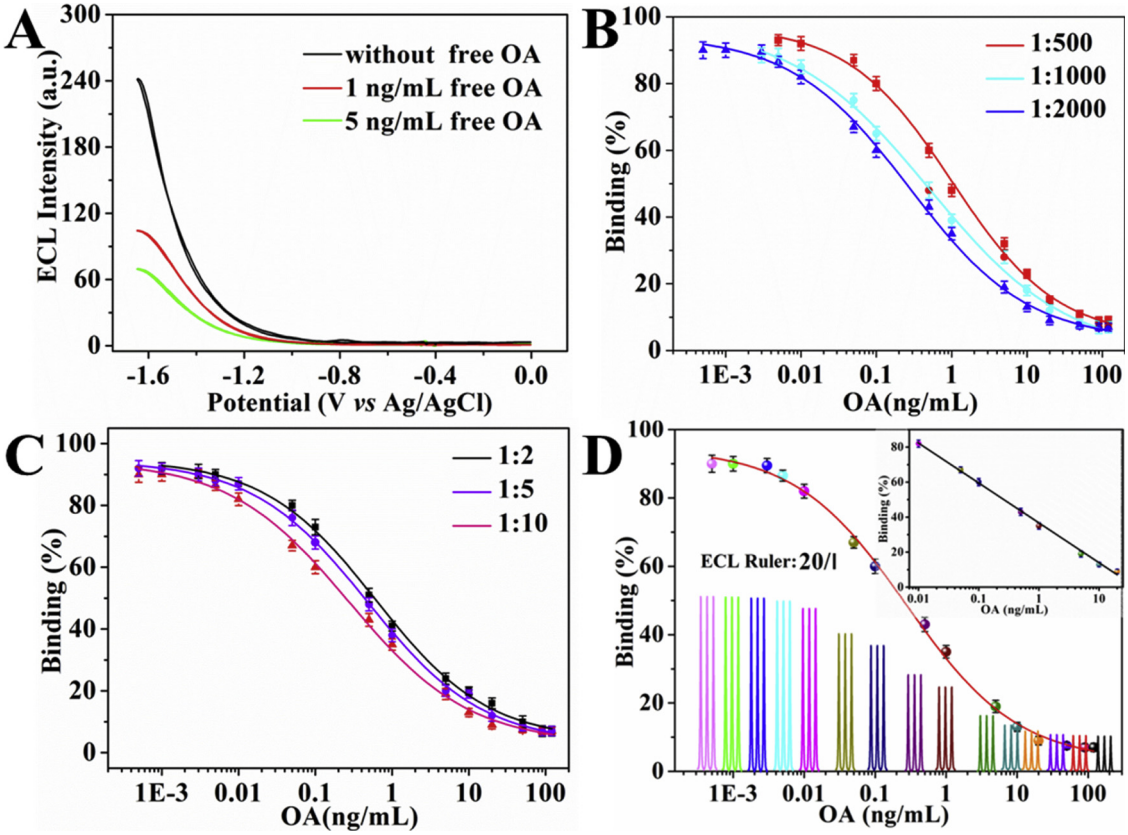

Fig. 5. (A) I_{ECL}-E curves of OA-CMCNT-PDDA-AuNCs GCE incubated in P, S-GQDs-Ab solution without and with 1 ng mL^{-1} and 5 ng mL^{-1} of OA, respectively. (B) Effect of the dilution ratio of anti-OA-MAb and (C) P, S-GQDs-MAb on the sensing performance. (D) The ECL curves and the corresponding calibration curve for OA obtained on the proposed immunoassay. The symbol "|" in 'ECL ruler: 20/|" represents as ECL intensity of 20 a.u.".

calculation was adopted to optimize the amount of P, S-GQDs-Ab, and the curve parameters derived from regression curves are summarized in Table S1. Considering both the signal intensity and sensitivity of the ECL immunosensor, the most suitable dilution ratio for anti-OA-MAb and P, S-GQDs-Ab was 1:2000 and 1:10, respectively.

Under the optimized conditions, the indirect competitive ECL immunoassay was performed to determine the OA concentration. Fig. 5D illustrates the ECL results and the corresponding calibration curve obtained by the developed system. As shown, the percentage of P, S-GQDs-Ab binding with the immobilized OA decreased proportionally with the concentration of free OA in the range of 0.01–20 ng mL^{-1}, and the LOD value (corresponding to 85% binding) was determined to be 0.005 ng mL^{-1}. As presented in the inset of Fig. 5D, the corresponding linear regression equation was y = -9.93 ln(x) + 36.42, with a correlation coefficient of 0.9978. Furthermore, the ECL results show high stability, with a low relative standard deviation (RSD) of 1.3% between 15 curves (Fig. S5). Additionally, results obtained with the proposed ECL immunosensor exhibited a wider linear range and relative lower LOD values as compared to other OA immune-sensing methods, including electrochemical, fluorescence, and luminescence, as concluded in Table 1 [5,6,8–10,43,44]. The advanced performance of the ECL immunosensor was attributed to three factors: (i) P, S-GQDs with good ECL properties efficiently conjugated with anti-OA-MAb to form an advanced ECL probe; (ii) direct immobilization of OA via covalent linking to increase accessibility of OA towards P, S-GQDs-Ab; (iii) additional reactive sites provided by the CMCNT-PDDA-AuNCs composite for OA immobilization, which further improved the sensitivity of the OA immunosensor.

To investigate its repeatability and reproducibility, intra- and inter-assay precisions were calculated by monitoring three quality-controlled OA. For repeated (n = 6) determination of OA at 0.1, 0.5, and 1.0 ng mL^{-1}, the RSD values were 4.3, 4.1, and 3.7%, respectively. Fig. S6 showed the repeatability of the ECL immunosensor for detecting 1.0 ng mL^{-1} of OA for six times using an electrode. Further, the RSD values for the inter-assay (n = 6) were 6.5, 5.8, and 5.4%, respectively. Both of the intra- and inter-assay precisions were less than 10%, indicating good repeatability and reproducibility of the as-developed OA ECL immunosensor.

Table 1
Comparison of anatytical properties of various sensors for OA determination.

Method	Range (ng mL^{-1})	LOD (ng mL^{-1})	Reference
DPV	0.78-500	0.5	43
DPV	1-300	0.55	6
Impedance	0.195-12.5	0.3	9
Impedance	0.1-60	0.07	10
Amperometry	0.19-25	0.15	44
CL-ELISA	0.03-0.2	-	5
Fluorescence	0.1-50	0.05	8
ECL	0.01-20	0.005	This work

Furthermore, the specificity and selectivity of the OA immunosensor were evaluated by comparing ECL signals of OA with dinophysistoxin-1 (DTX-1), 13-desmethyl spirolide C (SPX-1), and saxitoxin diacetate salt (STX) (at concentrations of 0.5 ng mL^{-1} for each toxin). The chemical structures of the above toxins are depicted in Fig. S7. From Fig. S8, the ECL intensity of DTX-1 was significantly reduced, while no obvious changes were observed for SPX-1 and STX. Similar results were obtained by adding OA to the above-mentioned toxins, further confirming the as-prepared OA immunoassay displayed no cross-reactivity towards SPX-1 and STX. However, the similar structures of OA and DTX-1, which both belong to the DSP toxin family, resulted in relatively high cross-reactivity of the proposed OA immunoassay towards DTX-1. Even

Table 2
Results obtained by the proposed ECL immunoassay and commercial OA ELISA kit for spiked *Ostrea plicatula* samples.

Sample	Spiked OA ($ng\,mL^{-1}$)	ELISA			This work		
		Found ($ng\,mL^{-1}$)	Recovery (%)	RSD (%)	Found ($ng\,mL^{-1}$)	Recovery (%)	RSD (%)
Ostrea plicatula	0.200	0.191	95.5	3.9	0.196	98.0	2.7
	0.400	0.422	105.5	4.3	0.391	97.8	3.2
	0.800	0.769	96.1	4.7	0.816	102.0	3.7

though, aprevious report pointed out that the toxic equivalency factors of both OA and DTX-1 were 1 [45]. Therefore, the as-developed OA immunoassay is applicable to monitor the safety level of shellfish.

3.4. Real sample analysis

To verify the feasibility for practical application, the proposed ECL immunosensor was applied to detect OA in mussel samples. The pretreatment procedures are described in the Experimental Methods. The recovery tests were carried out by spiking known amounts of OA in non-contaminated mussel samples, and the results were calculated based on the calibration curve presented in Fig. 5D. As summarized in Table 2, the detected values of OA agreed well with the corresponding spiked values. The recoveries varied from 97.8% to 102.0%, suggesting the low matrix effect of the immunoassay. In addition, the recoveries of the immunoassay were more favorable than those obtained from OA ELISA kits (95.5% to 105.5%), further confirming the superiority of the proposed OA immunoassay.

4. Conclusion

In summary, we for the first time, synthesized water-dispersed, uniform-sized P, *S*-GQDs by an electrolysis method and demonstrated their advance ECL properties. Based on systematically studies, a novel competitive indirect ECL immunosensor was fabricated for highly sensitive detection of OA using CMCNT-PDDA-AuNCs GCE as a sensing platform and P, S-GQDs as efficient ECL markers. Our results showed that the IC_{50} of the immunosensor was $0.25\,ng\,mL^{-1}$, and the linear range was $0.01–20\,ng\,mL^{-1}$ with a low detection limit of $0.005\,ng\,mL^{-1}$. As compared to traditional OA ELISA kits, our design revealed greater convenience, higher sensitivity response, and lower matrix effect. These advantages make the proposed ECL immunosensor promising for OA determination in mussel samples. Although this system mainly focused on OA detection, the strategy of using P, S-GQDs as ECL markers is a practical approach for fabricating high-performance ECL sensors to monitor other analytes.

Declaration of Competing Interest

There are no conflicts of interest to declare.

Acknowledgements

This work was financially supported by the National Natural Science Foundation of China (21675062), the National Key R&D Program of China (2018YFD0901004), the Science and Technology Planning Project of Fujian Province, China (2018D0019).

Appendix A. Supplementary data

Supplementary material related to this article can be found, in the online version, at doi:https://doi.org/10.1016/j.snb.2019.127383.

References

[1] S. Ramalingam, R. Chand, C.B. Singh, A. Singh, Phosphorene-gold nanocomposite based microfluidic aptasensor for the detection of okadaic acid, Biosens. Bioelectron. 135 (2019) 14–21.
[2] X. Zhang, J.R. Fang, L. Zou, Y.C. Zou, L. Lang, F. Gao, N. Hu, P. Wang, A novel sensitive cell-based love wave biosensor for marine toxin detection, Biosens. Bioelectron. 77 (2016) 573–579.
[3] C. Lin, Z.S. Liu, D.X. Wang, H.L. Ren, Y.S. Li, P. Hu, Y. Zhou, Y.P. Guo, X.M. Meng, S.Y. Lu, Sensitive and reliable micro-plate chemiluminescence enzyme immunoassay for okadaic acid in shellfish, Anal. Methods 6 (2014) 7142–7148.
[4] EFSA, Marine biotoxins in shellfish-okadaic acid and analogues. Scientific opinion of the panel on contaminants in the food chain, EFSA J. 589 (2008) 1–62.
[5] M.M. Vdovenko, C.T. Hung, I.Y. Sakharov, F.Y. Yu, Determination of okadaic acid in shellfish by using a novel chemiluminescent enzyme-linked immunosorbent assay method, Talanta 116 (2013) 343–346.
[6] J. Zhou, X.X. Qiu, K.Q. Su, G.X. Xu, P. Wang, Disposable poly (o-aminophenol)-carbon nanotubes modified screen print electrode-based enzyme sensor for electrochemical detection of marine toxin okadaic acid, Sens. Actuator. B Chem. 235 (2016) 170–178.
[7] B. Molinero-Abad, L. Perez, D. Izquierdo, I. Escudero, M.J. Arcos-Martinez, Sensor system based on flexible screen-printed electrodes for electrochemical detection of okadaic acid in seawater, Talanta 192 (2018) 347–352.
[8] S.J. Wu, N. Duan, H. Zhang, Z.P. Wang, Simultaneous detection of microcysin-LR and okadaic acid using a dual fluorescence resonance energy transfer aptasensor, Anal. Biochem. 407 (2015) 1303–1312.
[9] A. Hayat, L. Barthelmebs, J.L. Marty, Electrochemical impedimetric immunosensor for the detection of okadaic acid in mussel sample, Sens. Actuator. B Chem. 171–172 (2012) 810–815.
[10] S. Eissa, A. Ng, M. Siaj, A.C. Tavares, M. Zourob, Selection and identification of DNA aptamers against okadaic acid for biosensing application, Anal. Chem. 85 (2013) 11794–11801.
[11] S. Eissa, M. Zourob, A graphene-based electrochemical competitive immunosensor for the sensitive detection of okadaic acid in shellfish, Nanoscale 4 (2012) 7593–7599.
[12] Y.P. Dong, J. Wang, Y. Peng, J.J. Zhu, A novel aptasensor for lysozyme based on electrogenerated chemiluminescence resonance energy transfer between luminol and silicon quantum dots, Biosens. Bioelectron. 94 (2017) 530–535.
[13] H. Ke, H.F. Sha, Y.F. Wang, W.W. Guo, X. Zhang, Z.M. Wang, C.S. Huang, N.Q. Jia, Electrochemiluminescence resonance energy transfer system between GNRs and Ru $(bpy)_3^{2+}$: Application in magnetic aptasensor for β-amyloid, Biosens. Bioelectron. 100 (2018) 266–273.
[14] L. Tan, J.J. Ge, M. Jiao, G.F. Jie, S.Y. Niu, Amplified electrochemiluminescence detection of DNA based on novel quantum dots signal probe by multiple cycling amplification strategy, Talanta 183 (2018) 108–113.
[15] H. Zhang, C. Zhang, D. Liu, F.M. Zuo, S.H. Chen, R. Yuan, W.J. Xu, A ratiometric electrochemiluminescent biosensor for Con A detecting based on competition of dissolved oxygen, Biosens. Bioelectron. 120 (2018) 40–46.
[16] B. Martín-García, Y. Bi, M. Prato, D. Spirito, R. Krahne, G. Konstantatos, I. Moreels, Reduction of moisture sensitivity of PbS quantum dot solar cells by incorporation of reduced graphene oxide, Sol. Energ. Mat. Sol. C. 183 (2018) 1–7.
[17] Z.F. Liu, Z.H. Chen, Fei Yu, Microencapsulated phase change material modified by graphene oxide with different degrees of oxidation for solar energy storage, Sol. Energ. Mat. Sol. C. 174 (2018) 453–459.
[18] T. Soltani, A. Tayyebi, B.K. Lee, Efficient promotion of charge separation with reduced graphene oxide (rGO)in BiVO4/rGO photoanode for greatly enhanced photoelectrochemical watersplitting, Sol. Energ. Mat. Sol. C. 185 (2018) 325–332.
[19] Y. Tang, J.J. Li, Q.F. Guo, G.M. Nie, An ultrasensitive electrochemiluminescence assay for Hg^{2+} through graphene quantum dots and poly(5-formylindole) nanocomposite, Sens. Actuator. B Chem. 282 (2019) 824–830.
[20] G.T. Jie, Q. Zhou, G.F. Jie, Graphene quantum dots-based electrochemiluminescence detection of DNA using multiple cyclingamplification strategy, Talanta 194 (2019) 658–663.
[21] L.Y. Zheng, Y.W. Chi, Y.Q. Dong, J.P. Lin, B.B. Wang, Electrochemiluminescence of water-soluble carbon nanocrystals released electrochemically from graphite, J. Am. Chem. Soc. 131 (2009) 4564–4565.
[22] R.Z. Zhang, J.R. Adsetts, Y.T. Nie, X.H. Sun, Z.F. Ding, Electrochemiluminescence of nitrogen- and sulfur-doped graphene quantum dots, Carbon 129 (2018) 45–53.
[23] C.Q. Wang, J. Qian, K. Wang, M.J. Hua, Q. Liu, N. Hao, T.Y. You, X.Y. Huang, Nitrogen-doped graphene quantum dots@SiO_2 nanoparticles as electrochemiluminescence and fluorescence signal indicators for magnetically-controlled

aptasensor with dual detection channels, ACS Appl. Mater. Inter. 7 (2015) 26865–26873.
[24] H.J. Chen, W. Li, Q. Wang, X. Jin, Z. Nie, S.Z. Yao, Nitrogen doped graphene quantum dots based single-luminophor generated dual-potential electrochemiluminescence system for ratiometric sensing of Co^{2+} ion, Electrochim. Acta 214 (2016) 94–102.
[25] S.F. Chen, X.Q. Chen, T.T. Xia, Q. Ma, A novel electrochemiluminescence sensor for the detection of nitroaniline based on the nitrogen-doped graphene quantum dots, Biosens. Bioelectron. 85 (2016) 903–908.
[26] M.L. Wang, Y.A. Sun, M.L. Yang, CdS QDs amplified electrochemiluminescence of N,S co-doped graphene quantum dots and its application for Pb(II) determination, Chem. Lett. 47 (2018) 44–47.
[27] R.J. Liu, J.J. Zhao, Z.R. Huang, L.L. Zhang, M.B. Zou, B.F. Shi, S.L. Zhao, Nitrogen and phosphorus co-doped graphene quantum dots as a nano-sensor for highly sensitive and selective imaging detection of nitrite in live cell, Sens. Actuator. B Chem. 240 (2017) 604–612.
[28] Zhang C.F, Y.Y. Cui, L. Song, X.F. Liu, Z.B. Hu, Microwave assisted one-pot synthesis of graphene quantum dots as highly sensitive fluorescent probes for detection of iron ions and pH value, Talanta 150 (2016) 54–60.
[29] M. Amatatongchai, W. Sroysee, S. Chairam, D. Nacapricha, Simple flow injection for determination of sulfite by amperometric detection using glassy carbon electrode modified with carbon nanotubes–PDDA–gold nanoparticles, Talanta 133 (2015) 134–141.
[30] B. Hemmateenejad, F. Shakerizadeh-Shirazi, F. Samari, BSA-modified gold nanoclusters for sensing of folic acid, Sens. Actuator. B Chem. 199 (2014) 42–46.
[31] Z. Zhang, N.F. Zhu, Y.M. Zou, X.Y. Wu, G.B. Qu, J.B. Shi, A novel, enzyme-linked immunosorbent assay based on the catalysis of AuNCs@BSA-induced signal amplification for the detection of dibutyl phthalate, Talanta 179 (2018) 64–69.
[32] A. Hayat, L. Barthelmebs, A. Sassolas, J.L. Marty, An electrochemical immunosensor based on covalent immobilization of okadaic acid onto screen printed carbon electrode via diazotization-coupling reaction, Talanta 85 (2011) 513–518.
[33] A. Sassolas, G. Catanante, A. Hayat, G. Catanante, A. Hayat, L.D. Stewart, C.T. Elliott, J.L. Marty, Improvement of the efficiency and simplification of ELISA tests for rapid and ultrasensitive detection of okadaic acid in shellfish, Food Control 30 (2013) 144–149.
[34] W.J. Wang, S.F. Xu, N. Li, Z.Y. Huang, B.Y. Su, X.M. Chen, Sulfur and phosphorus co-doped graphene quantum dots for fluorescent monitoring of nitrite in pickles, Spectrochim. Acta, A 221 (2019) 117211.
[35] S.H. Li, Y.C. Li, J. Cao, J. Zhu, L.Z. Fan, X.H. Li, Sulfur-doped graphene quantum dots as a novel fluorescent probe for highly selective and sensitive detection of Fe^{3+}, Anal. Chem. 86 (2014) 10201–10207.
[36] A. Ananthanarayanan, Y. Wang, P. Routh, M.A. Sk, A. Than, M. Lin, J. Zhang, J. Chen, H.D. Sun, P. Chen, Nitrogen and phosphorus co-doped graphene quantum dots: synthesis from adenosine triphosphate, optical properties, and cellular imaging, Nanoscale 7 (2015) 8159–8165.
[37] W.J. Wang, J.W. Peng, F.M. Li, B.Y. Su, X. Chen, X.M. Chen, Phosphorus and chlorine co-doped carbon dots with strong photoluminescence as a fluorescent probe for ferric ions, Microchim. Acta 186 (2019) 32.
[38] Y.M. Long, L. Bao, Y. Peng, Z.L. Zhang, D.W. Pang, Self-co-reactant and ion-annihilation electrogenerated chemiluminescence of carbon nanodots, Carbon 129 (2017) 168–174.
[39] L.L. Li, J. Ji, R. Fei, C.Z. Wang, Q. Lu, J.R. Zhang, L.P. Jiang, J.J. Zhu, A facile microwave avenue to electrochemiluminescent two-color graphene quantum dots, Adv. Funct. Mater. 22 (2012) 2971–2979.
[40] Y.P. Dong, G. Chen, Y. Zhou, J.J. Zhu, Electrochemiluminescent sensing for caspase 3 activity based on $Ru(bpy)_3^{2+}$-doped silica nanoprobe, Anal. Chem. 88 (2016) 1922–1929.
[41] G.C. Fan, L. Han, H. Zhu, J.R. Zhang, J.J. Zhu, Ultrasensitive photoelectrochemical immunoassay for matrix metalloproteinase-2 detection based on CdS:Mn/CdTe cosensitized TiO_2 nanotubes and signal amplification of SiO_2@Ab_2 Conjugates, Anal. Chem. 86 (2014) 12398–12405.
[42] D.P. Tang, J. Tang, B.L. Su, G.N. Chen, Gold nanoparticles-decorated amine-terminated poly(amidoamine) dendrimer for sensitive electrochemical immunoassay of brevetoxins in food samples, Biosens. Bioelectron. 26 (2011) 2090–2096.
[43] A. Hayat, L. Barthelmebs, A. Sassolas, J.L. Marty, Development of a novel label-free amperometric immunosensor for the detection of okadaic acid, Anal. Chem. Acta 724 (2012) 92–97.
[44] R.B. Dominguez, A. Hayat, A. Sassolas, G.A. Alonso, R. Munoz, J.L. Marty, Automated flow-through amperometric immunosensor for highly sensitive and on-line detection of okadaic acid in mussel sample, Talanta 99 (2012) 232–237.
[45] L.D. Stewart, C.T. Elliott, A.D. Walker, R.M. Curran, L. Connolly, Development of a monoclonal antibody binding okadaic acid and dinophysistoxins-1, -2 in proportion to their toxicity equivalence factors, Toxicon 54 (2009) 491–498.

Jiawei Peng is currently a M.S. student of the College of Food and Biological Engineering at Jimei University. His research is focused on GQDs-based electrochemiluminescence biosensors.

Zixuan Zhao is currently a M.S. student of the College of Food and Biological Engineering at Jimei University. His research is focused on electrochemical biosensors in food safety.

Minli Zheng is currently a M.S. student of the College of Food and Biological Engineering at Jimei University. Her research is focused on the synthesis of 3D materials for the sample pretreatment.

Bingyuan Su received his M.S. degree in Analytical Chemistry from Xiamen University in 2008. Currently, he is working as a supervising technician in Xiamen Center for Disease Control and Prevention, and his scientific interests focus on the areas of analytical chemistry and food safety.

Xiaomei chen is a Full Professor in the College of Food and Biological Engineering at Jimei University. She received her B.S. and Ph.D. degree from Xiamen University in 2005 and 2011, respectively. She worked as a JSPS postdoctor in Kyoto University in Prof. Oyama's lab during 2012-2014. *Her* scientific interests focus on solid-state electrochemiluminescence, carbon and metal nanomaterials for electrochemical and bioanalytical applications.

Xi Chen is a Full Professor in the Department of Chemistry at Xiamen University, China. He received his Ph.D. (1996) degree in Analytical Chemistry from Kyoto Institute of Technology, Japan. His research interests cover electrochemiluminescence, bio-chemical sensor and solid phase microextraction.